LBNL-51709

Precise Shell Effects and Barriers: a New Inroad to Fission Saddle Point Spectroscopy

L. Phair, L. G. Moretto, K. X. Jing, L. Beaulieu, D. Breus,
J. B. Elliott, T. S. Fan, Th. Rubehn, and G. J. Wozniak
Nuclear Science Division, Lawrence Berkeley National Laboratory,
University of California, Berkeley, California 94720

(Dated: November 8, 2002)

Abstract

Fission excitation functions have been measured for a chain of neighboring compound nuclei, from ^{207}Po to ^{212}Po. We present a new analysis which provides a determination of the fission barriers and ground state shell effects with nearly spectroscopic accuracy. The improved accuracy achieved in this analysis may lead to a future detailed exploration of the saddle mass surface and its spectroscopy. The sensitivity of the fission probabilities on shell effects extends to excitation energies of 150 MeV and negates recent claims for the disappearance of shell corrections due to collective effects.

PACS numbers: 24.75.+i, 25.85.Ge

The study of nuclei under extreme conditions (spin, isospin, temperature, and deformation) is a major theme of nuclear physics. Fission is a fertile testing ground of nuclei under extreme deformation for several reasons.

A fissioning nucleus allows us to explore the *most* extreme nuclear deformation associated with a stationary point, well beyond that of super- or even hyper-deformation. The saddle configuration is a bottleneck in phase space, a "stationary" point at which the probability to fission is determined. It is also able to sustain its own spectroscopy in the $N-1$ modes orthogonal to the fission mode. This spectroscopy begins with the saddle mass (M_s) which is simply the ground state mass (M_{gs}) plus the experimental fission barrier (B_f) [1]. The physics describing the saddle point ground and excited states should be similar to that of a deformed nucleus. Initial attempts at saddle point spectroscopy were made earlier in the low barrier actinide regions [2], but could not be extended to the much higher barriers of lighter elements.

Historically, experimental fission barriers in lighter nuclei have been disproportionately useful in fixing the adjustable parameters in theories of nuclear masses and deformabilities (such as the liquid drop model).

Shell effects in the ground state and at the saddle, pairing, congruence energy [4], single particle level densities are examples of quantities that should be immediately accessible when studying saddle properties.

Yet as important a testing ground as fission would seem to be, so far fission barriers and ground state shells have been measured only anecdotally and with only moderate accuracy [3]. The lack of precise and systematic data measured over a wide range of excitation energy has left the expectations mentioned above largely unfulfilled. In this letter we provide new precision data, systematically measured for an isotopic chain of Po compound nuclei, covering a large excitation energy range. We also describe a new analysis technique which results in fission barriers and ground state shell corrections with nearly spectroscopic accuracy.

The fission data were taken at the 88-Inch Cyclotron of the Lawrence Berkeley National Laboratory. We measured with high precision the fission excitation functions of the neighboring compound Po nuclei $^{207-212}$Po produced in ^{3}He- and ^{4}He-induced reactions on isotopically enriched Pb targets (see Fig. 1).

We chose these particular reactions for several reasons. First, the shell corrections and fission barriers in the Pb region are large and easy to measure. Second, the light ion induced

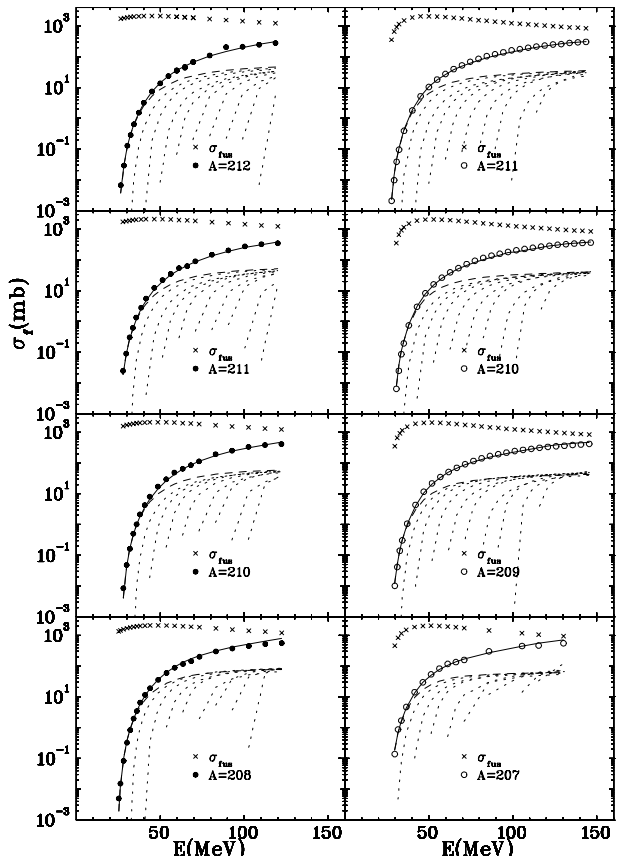

FIG. 1: The fission cross section (solid and open symbols) are plotted as a function of excitation energy for the indicated nuclei. The errors are smaller than the symbols. The dashed curve represents the first chance fission cross section. The dotted curves represent the second and higher chance fission cross sections. The solid curve is their sum, the total fission cross section. The left column contains α-induced reactions. The right contains ^{3}He-induced reactions. The fusion cross sections (cross symbols) are described in the text.

reactions have only modest amounts of angular momentum ($< 25\hbar$). The relevant rotational energies are small, ≈ 2 MeV for a spherical shape and ≈ 0.8 MeV for the saddle shape of a Po nucleus with an angular momentum of $20\hbar$. And third, there are four stable isotopes of Pb from which one can make clean targets.

Fission events were identified in two large area parallel plate avalanche counters. The experimental details are described in ref. [5]. The statistical errors of the measured fission cross sections σ_f are smaller than 2% for excitation energies above 50 MeV. And since the fissioning systems for different beam-target combinations were measured with the same detector setup, the relative systematic errors are estimated to be small ($\sim 4\%$).

The solid and open symbols in Fig. 1 represent the fission cross section data for neighboring compound nuclei. The ^{4}He-induced reactions are shown in the left column and the ^{3}He-induced reactions are shown in the right. In two cases ($A = 211, 210$), we have overlap points where the same compound nucleus was formed via two different entrance channels. The fission cross sections cover seven orders of magnitude for these reactions.

To determine the fission probability, we use standard transition state theory as applied in ref. [5] and calculate the fission decay width

$$\Gamma_f = \frac{1}{2\pi\rho(E)} \int \rho_f(E - B_f - \epsilon) d\epsilon \tag{1}$$

where ρ_f is the level density at the saddle, ϵ is the kinetic energy associated with the fission channel, and ρ is the level density of the compound nucleus.

We neglect charged particle emission, since fission following proton or α particle emission is known to be small for these reactions [6]. The width for neutron emission (the only other exit channel assumed in our analysis) is

$$\Gamma_n = \frac{2mR^2 g\prime}{\hbar^2} \frac{1}{2\pi\rho(E)} \int \epsilon \rho_d(E - B_n - \epsilon) d\epsilon. \tag{2}$$

where m denotes the neutron mass, R is the radius and ρ_d is the level density of the daughter nucleus after neutron emission, $g\prime$ is the spin factor (=2), B_n is the neutron binding energy, and ϵ is the kinetic energy of the neutron.

Using for simplicity the Fermi gas level density and taking into account the angular momentum a fissioning nucleus may have, Eqs. (1) and (2) can be evaluated and their ratio taken [7] so that Γ_f/Γ_n is

$$\frac{\Gamma_f}{\Gamma_n} = \frac{T_f - \frac{1}{2a_f}}{K\left(T_d^2 - \frac{3}{2a_d}T_d + \frac{3}{4a_d^2}\right)} \frac{\rho_f(E - B_f - E_r^s)}{\rho(E - B_n - E_r^{gs})} \tag{3}$$

where a_f and T_f denote the level density parameter and temperature at the saddle, a_d and T_d denote the level density parameter and temperature of the residual daughter after neutron emission, E_r^s and E_r^{gs} denote the rotational energy of the system at the saddle point and the energy of the rotating ground state and $K = 2mR^2 g\prime/\hbar^2$. The ground state and saddle moments of inertia were taken from Sierk [8].

Using for simplicity the Fermi gas level density, the ratio of the level densities in Eq. (3) becomes

$$\frac{\rho_f(E - B_f - E_r^s)}{\rho(E - B_n - E_r^{gs})} \propto e^{2\sqrt{a_f(E - B_f - E_r^s)} - 2\sqrt{a_d(E - B_n - E_r^{gs})}}. \tag{4}$$

For nuclei with strong shell effects, the approximation $\rho(E - B_n - E_r^{gs}) \propto \exp(2\sqrt{a_d(E - B_n - E_r^{gs})})$ becomes a poor one. The shell effects of a nucleus affect its level density in a rather complicated way at low energies. But at high enough excitation energies, we can use the asymptotic form $\rho(E) \propto \exp(2\sqrt{a(E + \Delta_{\rm shell})})$ [9]. This approximation is particularly useful for Γ_n where the excitation energy is always at least 5 MeV above the fission barrier (i.e., approximately 25-30 MeV). On the other hand, at the saddle no shell effects are expected much larger than 1 MeV.

For the daughter nucleus produced by neutron emission, the level density takes the asymptotic form:

$$\rho_d(E - B_n - E_r^{gs}) \propto \exp\left(2\sqrt{a_d(E - B_n - E_r^{gs} + \Delta_{\rm shell}^{n-1})}\right) \tag{5}$$

where $\Delta_{\rm shell}^{n-1}$ is the ground state shell effect of the daughter nucleus after neutron emission.

For the saddle level density (ρ_f), the problems should be far less serious. On the one hand, the large deformations at the saddle point imply small shell effects there. On the other hand, topologically the saddle point should be located between regions of positive and negative shell effects, thus substantially limiting the saddle point shell corrections [10].

Pairing affects the level density in a manner similar to the shell effects. The level density is evaluated at an energy shifted by the condensation energy ΔE_c. The condensation energies are calculated separately for protons and neutrons. For an even-even nucleus, $\Delta E_c = \frac{1}{2}g_n\Delta_n^2 + \frac{1}{2}g_p\Delta_p^2$, where $g_n = (3/\pi^2)a_n$, $g_p = (3/\pi^2)a_p$, and $a_d = a_n + a_p = N/8.5\ \mathrm{MeV}^{-1} + Z/8.5\ \mathrm{MeV}^{-1} = A/8.5\ \mathrm{MeV}^{-1}$. In general,

$$\Delta E_c = \frac{1}{2}g_n\Delta_n^2 + \frac{1}{2}g_p\Delta_p^2 - \mathrm{mod}(N,2)\Delta_n - \mathrm{mod}(Z,2)\Delta_p. \tag{6}$$

The ground state gap parameters for protons (Δ_p) and for neutrons (Δ_n) were chosen to be

$$\Delta_p = \Delta_n = \frac{12\mathrm{MeV}}{\sqrt{A}}. \tag{7}$$

At the saddle, the gap parameter for the neutrons(Δ_n^f) was taken to be $\Delta_n^f = S\exp\left(-1/g_n^f G\right)$ where S and G were chosen to reproduce the ground state values (Eq. (7)) and $g_n^f = (3/\pi^2)(N/A)a_f$. A similar expression for Δ_p^f can be calculated for protons using $g_p^f = (3/\pi^2)(Z/A)a_f$. Consequently the condensation energy at the saddle we express as

$$\Delta E_c^s = \frac{1}{2}g_n^f(\Delta_n^f)^2 + \frac{1}{2}g_p^f(\Delta_p^f)^2 - \mathrm{mod}(N,2)\Delta_n^f - \mathrm{mod}(Z,2)\Delta_p^f \tag{8}$$

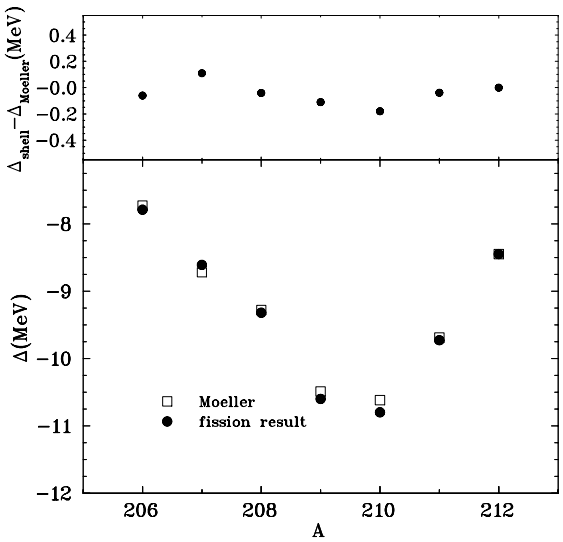

FIG. 2: The shell corrections from the fission fits (solid circles) and the shell corrections from Möller *et al.* [11] are plotted as a function of mass number for Po. The residual difference between the two data sets is shown in the upper panel.

The resulting expression for Γ_f/Γ_n is

$$\frac{\Gamma_f}{\Gamma_n} \propto e^{2\sqrt{a_f\left(E-B_f-E_r^s-\Delta E_c^f\right)}-2\sqrt{a_d\left(E-B_n-E_r^{gs}+\Delta_{\rm shell}^{n-1}-\Delta E_c\right)}} \tag{9}$$

We further assume that the fission barrier can be broken into two parts: $B_f = B_{\rm macro} - \Delta_{\rm shell}$ where for the macroscopic part ($B_{\rm macro}$) we take a scaled value of the Thomas-Fermi predictions [1], and the microscopic part is the ground state shell correction.

The expression for Γ_f/Γ_n (Eq. (9)) has four free parameters: $B_{\rm macro}$, $\Delta_{\rm shell}$ of the fissioning system, $\Delta_{\rm shell}^{n-1}$ of the 1 neutron out daughter nucleus, and the ratio of the level density parameters a_f/a_d.

To make use of this description of Γ_f/Γ_n, we write the total fission cross section as

$$\sigma_f = \sum_{i=0} \sigma_f^{(i)} = \sum_{l=0}^{l=l_{\rm max}} \sum_{i=0} \sigma_l P_f^{(i)}(E,l) \tag{10}$$

where $\sigma_f^{(i)}$ is the fission cross section after i neutrons have been emitted, σ_l is the angular momentum distribution of the fusion cross section ($(2l+1)\pi\lambda\!\!\!^{-2}$), $l_{\rm max}$ comes from the fusion cross sections (crosses in Fig. 1) and $P_f^{(i)}(E,l)$ is the fission probability after the emission of i neutrons from a compound nucleus of initial angular momentum l and initial energy E.

The fission probability at each "step" i can be written as

$$P_f^{(i)}(E,l) = \frac{1}{1+\frac{\Gamma_n}{\Gamma_f}(E,l,i)} \tag{11}$$

where the angular momentum dependence comes in through the rotational energy dependence of Γ_f/Γ_n and the "multiple-chance" energy dependence is accounted for on average by assuming that with the emission of each neutron, the excitation energy drops by $2T + B_n$.

With Eqs. (3), and (9)-(11), we are prepared to fit any chain of neighboring isotope fission data. However, a remark regarding the fusion cross sections is in order. If we use the Bass model description of the fusion cross sections [12] and fit the fission cross sections with the method outlined above, we get reasonable fits to the α-induced reactions, but somewhat poorer fits for the ^{3}He-induced reactions. The Bass model may not describe well both the ^{3}He- and ^{4}He-induced fusion cross sections. Therefore, we have chosen to leave the fusion cross section as a free parameter constrained to the form:

$$\sigma_0 = \frac{E_2 - V}{E_{cm}} \pi R^2 \tanh\left(\frac{E_{cm} - V}{E_2 - V}\right) \tag{12}$$

where V represents the fusion barrier, πR^2 is a geometric cross section and $E_2 = 1/2\mu v_{\rm rel}^2$, the energy above which the fusion cross section effectively falls like $1/E_{cm}$. Note that in the low energy limit ($E_{cm} \approx V$), Eq. (12) goes to

$$\sigma_0 = \pi R^2 \left(1 - \frac{V}{E_{cm}}\right) \tag{13}$$

and at high energies σ_0 goes to

$$\sigma_0 = \frac{E_2 - V}{E_{cm}} \pi R^2. \tag{14}$$

With this choice of fusion cross sections we are ready to proceed and fit the fission cross sections. Note that this new fitting technique requires a self-consistent global description of the data. For example, the third chance fission for nucleus A uses the same fission barrier as the second chance fission of nucleus $A-1$, which is the same barrier as first chance fission of nucleus $A-2$.

The total fission cross sections calculated using Eq. (10) are shown as the solid lines in Fig. 1. The dashed line represents "first-chance" fission. The dotted lines represent second, third and higher chance fission yields.

To fit all of the systems in Fig. 1, eleven free parameters were taken: three to describe the fusion cross sections ($v_{\rm rel}$ and one R for each projectile type, see Eq. (12)), one to describe

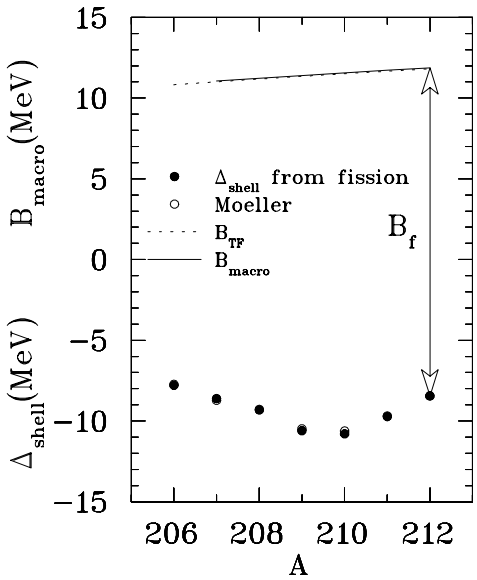

FIG. 3: The shell corrections extracted from the fission fits (solid circles) are plotted as a function of mass number. The open circles represent the ground state shell correction estimated by Möller *et al.* [11]. The solid line is the macroscopic barrier extracted from the fission fit and the dashed line is a Thomas-Fermi estimate [1]. The difference between the the macroscopic barrier $B_{\rm macro}$ and the shell correction $\Delta_{\rm shell}$ is the fission barrier B_f.

the A dependence of the macroscopic barriers, one to describe the average value of a_f/a_d, and one each to describe the six shell corrections for the 1n daughter channel of the six fissioning systems (the shell correction for ^{212}Po was fixed at the Möller value [11]).

The extracted $\Delta_{\rm shell}$ values are shown by the solid circles in Fig. 2. They show a clear shell closure at $A = 210$ ($N = 126$). Furthermore, there is a remarkable agreement between the values from the present fission analysis and those determined by Möller *et al.* in fitting the ground state masses [11] (open squares). The mean deviations are smaller than 200 keV (upper panel of Fig 2).

The agreement is remarkable, especially compared to earlier attempts [3] (fitting one compound system at a time using a "first-chance-emission only" formalism) where the uncertainties were typically ±1.5 MeV. The errors from the present analysis suffer from a lack of exact knowledge of the fusion cross section, a value of a_f/a_d, and $B_{\rm macro}$. Because these three parameters are so strongly correlated, the chi square space of the fit is extremely flat and the resulting error matrix is not positive-definite. Consequently, errors from the full fit cannot be assigned. However, if values for the fusion cross section, a_f/a_d, and $B_{\rm macro}$ are

"frozen" to their best values and the fits repeated with only the shell corrections free, the resulting calculated errors are less than 10 keV.

Furthermore, the extraction of shell corrections from the fission fits offers an alternative way to measure shell effects which is purely local, i.e. it does not depend on the (assumed) liquid drop background.

These shell effects modify the fission probability according to Eq. (9) up to the highest excitation energies ($\approx$ 150 MeV). This observation is at variance with recent claims of loss of shell structure at high energies [13].

The extracted fission barriers are shown in Fig. 3 as a difference between the shell correction and the macroscopic barriers. The macroscopic barrier from the fit is given by the solid line and is nearly indistinguishable from the Thomas-Fermi prediction (solid line) [1]. With data at other fissilities, it should be possible to explore systematic changes in the macroscopic barriers, in particular the shape changes of the congruence energy predicted by Myers and Swiatecki [4].

The ratio a_f/a_d has an average value of ≈ 1.02. With additional data at other values of fissility, it should be possible to study the surface area dependence of a_f [14].

In summary, we have reported new precision fission data, and we have extracted accurate fission barriers and ground state shell corrections with a new method of globally fitting fission data for an isotopic chain of nuclei. An accurate description of the saddle mass configuration may open avenues that have been explored extensively for ground state masses. For example, it may soon be possible to address pairing corrections at the saddle, the surface area (or fissility) dependence of both the saddle level density and the macroscopic barrier, and even shell effects at the saddle in a quantitative fashion. As more data become available, especially at the new radioactive beam facilities, the techniques presented here may prove valuable for an accurate description and understanding of the fission "saddle-mass" surface.

This work was supported by the US Department of Energy.

[1] W.D. Myers and W.J. Swiatecki, Phys. Rev. C **60**, 4606 (1999).

[2] See the review by Cyriel Wagemans, *The Nuclear Fission Process*, (CRC Press, Boston 1991).

[3] L.G. Moretto, *et al.*, Phys. Rev. Lett. **75**, 4186 (1995).

[4] W.D. Myers and W.J. Swiatecki, Nucl. Phys. A **612**, 249 (1997).

[5] Th. Rubehn, *et al.*, Phys. Rev. C **54**, 3062 (1996).

[6] K. X. Jing, *et al.*, Phys. Lett. B **518**, 221 (2001).

[7] K. X. Jing, Ph.D Thesis, University of California at Berkeley, (1999); LBNL-43410.

[8] A. Sierk, private communication.

[9] J. R. Huizenga and L. G. Moretto, Ann. Rev. Nucl. Phys. **22**, 427 (1972).

[10] W.D. Myers and W.J. Swiatecki, Nucl. Phys. A **601**, 141 (1996).

[11] P. Möller, *et al.*, At. Data Nucl. Data Tab. **59**, 185 (1995).

[12] R. Bass, Phys. Rev. Lett. **39**, 265 (1977).

[13] A. R. Junghans, *et al.*, Nucl. Phys. A **629**, 635 (1998).

[14] J. Toke and W.J. Swiatecki, Nucl. Phys. A **372**, 141 (1981).